The generation of 150 km echoes through nonlinear wave mode coupling

William J. Longley[1]

[1]Center for Solar-Terrestrial Research, New Jersey Institute of Technology, Newark, NJ, USA

Corresponding author: William Longley (william.longley@njit.edu)

Key Points:

- A kinetic theory is developed to explain how Langmuir and Upper-Hybrid waves couple nonlinearly to ion-acoustic waves
- Nonlinear mode coupling solves the problem of how 150-km radar echoes are generated in the lower ionosphere
- Mode coupling explains why only lower frequency (30-50 MHz) radars observe the enhanced ion-acoustic waves in 150-km echoes

Abstract

A fundamental problem in turbulence is understanding how energy cascades across multiple scales. In this paper, a new weak turbulence theory is developed to explain how energy can be transferred from Langmuir and Upper-Hybrid waves (~10 MHz frequencies, 20-cm wavelengths) to ion-acoustic waves (~kHz frequencies, 3-meter wavelengths). A kinetic approach is used where the electrostatic Boltzmann equations are Fourier-Laplace transformed, and the nonlinear term is retained. A unique feature of this approach is the ability to calculate power spectra at low frequencies, for any wavelength or angle to the magnetic field. The results of this theory explain how 150-km echoes are generated in the ionosphere. First, peaks in the suprathermal electron velocity distribution drive a bump-on-tail like instability. This instability excites the Upper-Hybrid mode, and the nonlinear mode coupling theory shows that the instability generates a ~10 dB enhancement of the ion-acoustic mode: matching the observed enhancement in 150-km echoes.

Plain Language Summary

The onset and evolution of turbulent flows is one of the most important outstanding questions in classical physics. When a fluid, gas, or plasma goes turbulent the flow can no longer be described with simple parameters such as speed and temperature. The fundamental problem is that these types of parameters describe the whole system, but during turbulence the flow is irregular and involves both microscopic and macroscopic motions. The research presented here shows how a macroscopic instability can drive microscopic changes at vastly different length and time scales. The approach taken falls into the category of weak-turbulence theory, which is where the turbulence is not overpowering, and therefore can be described using some of the standard tools from gas dynamics. This new turbulence theory is applied to the problem of 150-km echoes. These echoes are a plasma instability observed by radars in the lower ionosphere between 130-170 km in altitude. The mechanism of the plasma instability driving 150-km radar echoes has previously been worked out, but the weak-turbulence theory developed here is needed to fully explain the observations. The results provide an unprecedented description of plasma turbulence across multiple time and length scales.

1 Introduction

Kinetic plasma theory is built on a foundation of linearizing the Boltzmann equation and finding solutions algebraically. This technique has been highly successful in describing kinetic phenomena such as Landau damping (*Nicholson*, 1983) and instability growth rates (*Longley et al.*, 2020). However, linear theory assumes the plasma is near equilibrium, with only small perturbations occurring. This assumption makes it impossible for different wave modes to interact with each other, limiting its application to studies of turbulence and instabilities. In this paper, a nonlinear kinetic theory is developed to explain how two different wave modes can interact.

The motivation of this study is to explain the phenomenon of 150-km echoes, but the results apply to a broad range of nonlinear phenomenon. 150-km echoes are 10-20 dB enhancements of the ion-acoustic mode routinely observed at altitudes of 130-170 km by Jicamarca and other equatorial radars. *Chau et al.* (2023) provides a review of the observational history of 150-km echoes and the open questions surrounding them. The biggest open question is the simplest: How are 150-km echoes generated? Some recent progress has been made towards understanding the generation mechanism. *Oppenheim and Dimant* (2016), *Longley et al.* (2020, 2021), and *Green et al.* (2023) developed theory and simulations to show how peaks in the photoelectron distribution can drive a bump-on-tail-like instability at the same locations that 150-km echoes are observed, but they did not provide a complete explanation of their generation mechanism.

Figure (1) illustrates the outstanding problem of what is needed to generate 150-km echoes. The Upper-Hybrid mode is excited by the photoelectron driven Upper-Hybrid instability at high frequencies (~4 MHz) and short wavelengths ($\lambda = 20 - 40\ cm$) through a bump-on-tail like mechanism. However, observations of 150-km echoes are made at the much lower ion-acoustic mode frequencies (~kHz), and wavelengths of 3-meters or larger. Therefore, it must be explained how the energy from the instability converts to energy in the observed ion-acoustic mode. This model does that.

The goal of this paper is to describe how the high frequency instability developed in *Longley et al*. (2020, 2021) can couple nonlinearly to the low frequency ion-acoustic mode. Section 2 describes the theoretical derivation of the nonlinear mode coupling. Section 3 shows how it is applied to the problem of 150-km echoes, giving a complete explanation of how they are generated. Finally, Section 4 describes the limitations and future directions of this theoretical approach.

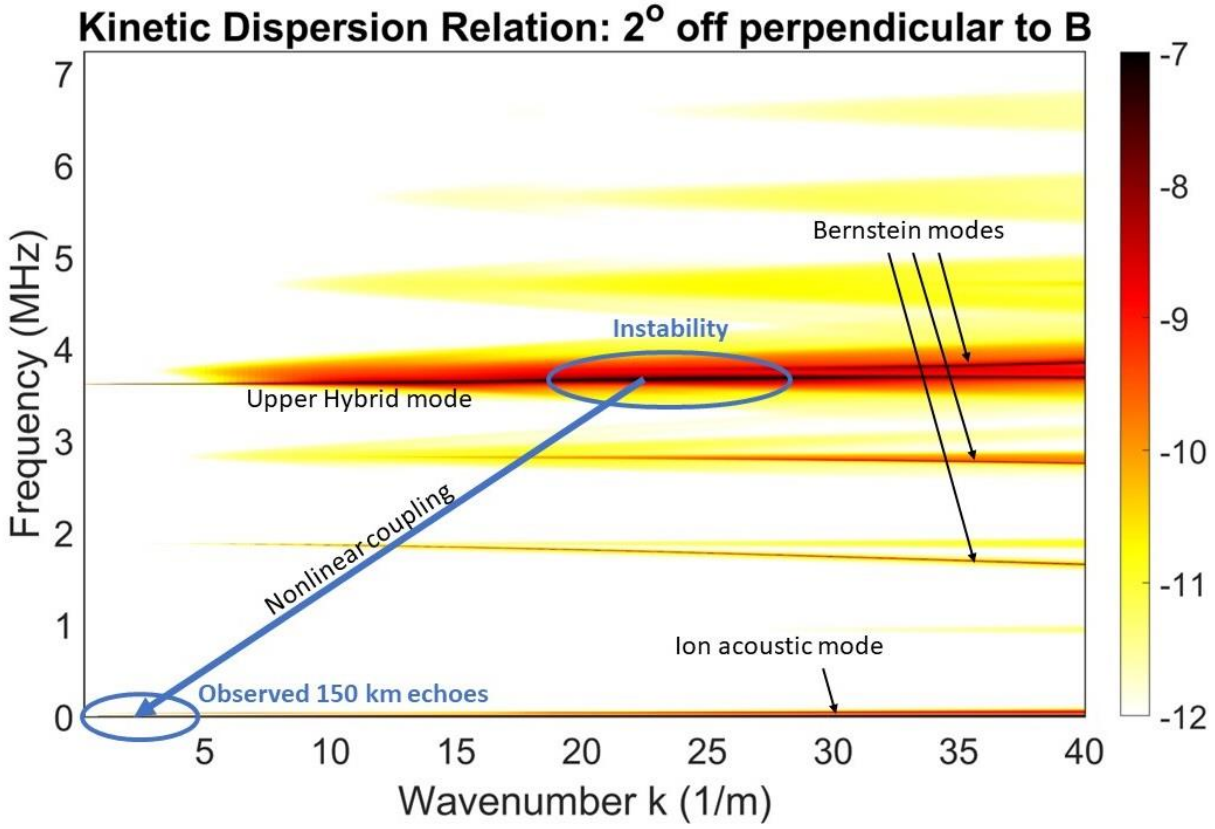

Figure 1. The kinetic dispersion relation using the theory in *Longley et al.* (2021). At an angle almost perpendicular to the magnetic field, the Upper-Hybrid mode is the most prominent feature at high frequencies (~4 MHz). The Upper-Hybrid mode is driven unstable by peaks in the photoelectron distribution. However, 150 km echoes are observed at lower frequencies (~kHz) and larger wavelengths. The theory developed in this paper describes how the instability at high frequencies couples nonlinearly to the low frequency waves, as shown by the blue arrow.

2 Derivation of Nonlinear Theory

2.1 Linear vs. Nonlinear Theory

To understand the need for a nonlinear solution of the Boltzmann equation, we first start with a typical linear solution. The Boltzmann equation is a general description of kinetic plasma behavior:

$$\frac{\partial F_s[t,\vec{x},\vec{v}]}{\partial t} + \vec{v}\cdot\nabla_x F_s[t,\vec{x},\vec{v}] + \frac{q_s}{m_s}\left(\vec{E}[t,\vec{x}] + \vec{v}\times\vec{B}\right)\cdot\nabla_v F_s[t,\vec{x},\vec{v}] = S[t,\vec{x},\vec{v}]. \#(1)$$

Physically, the Boltzmann equation is a total time derivative of the distribution function $F_s[t,\vec{x},\vec{v}]$ on the left-hand side, with a collision operator S on the right-hand side. In this paper the convention is used such that $F_s = n_s f_s$, and f_s is the normalized distribution function such that $\int d\vec{v}^3 f_s = 1$.

The process of linearization is to assume each variable quantity can be decomposed into a 0^{th} order term, and a small 1^{st} order perturbation:

$$F_s = F_{0s} + F_{1s}, \#(2)$$

$$\vec{E} = \vec{E}_0 + \vec{E}_1, \#(3)$$

$$\vec{B} = \vec{B}_0 + \vec{B}_1. \#(4)$$

We assume that $E_0 = 0$ for this solution. In the ionosphere, the Earth's magnetic field is strong enough that the electrostatic approximation is made, taking $\vec{B}_1 = 0$. Putting Equations 2 – 4 into Equation 1 produces

$$\frac{\partial}{\partial t}(F_{0s}[t,\vec{x},\vec{v}] + F_{1s}[t,\vec{x},\vec{v}]) + \vec{v}\cdot\nabla_x(F_{0s}[t,\vec{x},\vec{v}] + F_{1s}[t,\vec{x},\vec{v}]) + \frac{q_s}{m_s}\left(\vec{E}_1[t,\vec{x}] + \vec{v}\times\vec{B}_0\right) \cdot \nabla_v(F_{0s}[t,\vec{x},\vec{v}] + F_{1s}[t,\vec{x},\vec{v}]) = S[t,\vec{x},\vec{v}].$$

$$\#(5)$$

All the 0^{th} order terms can be collected together:

$$\left\{\frac{\partial F_{0s}[t,\vec{x},\vec{v}]}{\partial t} + \vec{v}\cdot\nabla_x F_{0s}[t,\vec{x},\vec{v}] + \frac{q_s}{m_s}\left(\vec{v}\times\vec{B}_0\right)\cdot\nabla_v F_{0s}[t,\vec{x},\vec{v}]\right\} + \left\{\frac{\partial F_{1s}[t,\vec{x},\vec{v}]}{\partial t} + \vec{v}\cdot\nabla_x F_{1s}[t,\vec{x},\vec{v}] + \frac{q_s}{m_s}\vec{E}_1[t,\vec{x}]\cdot\nabla_v F_{0s}[t,\vec{x},\vec{v}] + \frac{q_s}{m_s}\left(\vec{v}\times\vec{B}_0\right) \cdot\nabla_v F_{1s}[t,\vec{x},\vec{v}]\right\} + \frac{q_s}{m_s}\vec{E}_1[t,\vec{x}]\cdot\nabla_v F_{1s}[t,\vec{x},\vec{v}] = S[t,\vec{x},\vec{v}].$$

$$\#(6)$$

The zeroth order terms are simple and setting f_{0s} to an unchanging Maxwellian leads to the first set of brackets evaluating to 0. This leaves

$$\left\{\frac{\partial F_{1s}[t,\vec{x},\vec{v}]}{\partial t} + \vec{v}\cdot\nabla_x F_{1s}[t,\vec{x},\vec{v}] + \frac{q_s}{m_s}\vec{E}_1[t,\vec{x}]\cdot\nabla_v F_{0s}[\vec{v}] + \frac{q_s}{m_s}\left(\vec{v}\times\vec{B}_0\right)\cdot\nabla_v F_{1s}[t,\vec{x},\vec{v}]\right\} + \frac{q_s}{m_s}\vec{E}_1[t,\vec{x}]\cdot\nabla_v F_{1s}[t,\vec{x},\vec{v}] = S[t,\vec{x},\vec{v}].$$

$$\#(7)$$

Typically, the next step in solving for the density perturbations is to linearize Equation 7 by keeping only the first order terms (the bracketed terms). This linearization is justified by choosing the zeroth order distribution such that the first order distribution is a small perturbation, and since $E_1 \propto f_{1s}$ from Gauss' law, the term $\vec{E}_1\cdot\nabla_v f_{1s}$ is the product of two small quantities, and therefore is an even smaller quantity. Thus, only the terms in the brackets are retained, and the resulting equation is linear as it only contains single factors of f_{1s} or E_1.

The basis of the mode coupling developed here is to retain the nonlinear term, $\vec{E}_1\cdot\nabla_v f_{1s}$, in Equation 7. In the case of instability, the perturbed electric field can have significant amplitude and therefore the nonlinear term is no longer a small quantity.

2.2 The Fourier-Laplace Transform

We continue to follow the typical linear approach and Fourier-Laplace transform Equation 7, including the nonlinear term. In this paper we use the non-unitary convention for the Fourier transform, defined as

$$\hat{f}(k) = \int_{-\infty}^{\infty} f(x)\, e^{-ikx}\, dx\,. \#(8)$$

As discussed in texts such as *Nicholson* (1983), the time variable must be Laplace transformed instead of Fourier transformed in order to accommodate Landau damping. The convention we use for the Laplace transform is

$$\hat{f}(\omega) = \int_{0}^{\infty} f(t)\, e^{i(\omega - i\gamma)t} dt\,. \#(9)$$

In applying the Fourier-Laplace transform to Equation 7, the linear terms are straightforward and transform as

$$\frac{\partial F_{1s}[t,\vec{x},\vec{v}]}{\partial t} \Rightarrow -i(\omega - i\gamma)F_{1s}\left[\omega - i\gamma, \vec{k}, \vec{v}\right] - F_{1s}\left[t_0, \vec{k}, \vec{v}\right], \#(10)$$

$$\vec{v}\cdot\nabla_x F_{1s}[t,\vec{x},\vec{v}] \Rightarrow i\left(\vec{k}\cdot\vec{v}\right)F_{1s}\left[\omega - i\gamma, \vec{k}, \vec{v}\right], \#(11)$$

$$\frac{q_s}{m_s}\vec{E}_1[t,\vec{x}]\cdot\nabla_v F_{0s}[\vec{v}] \Rightarrow \frac{q_s}{m_s}\vec{E}_1\left[\omega - i\gamma, \vec{k}\right]\cdot\nabla_v F_{0s}[\vec{v}], \#(12)$$

$$\frac{q_s}{m_s}\left(\vec{v}\times\vec{B}\right)\cdot\nabla_v F_{1s}[t,\vec{x},\vec{v}] \Rightarrow \frac{q_s}{m_s}\left(\vec{v}\times\vec{B}\right)\cdot\nabla_v F_{1s}\left[\omega - i\gamma, \vec{k}, \vec{v}\right]. \#(13)$$

In Equation 10 an initial value term results from the Laplace transform, as an integration by parts is used to evaluate the time derivative.

The Fourier-Laplace transforms in Equations 10 – 13 are straightforward because each term is linear, and therefore only one function of *t* or *x* is present. However, the nonlinear term in Equation 7 is a product of two functions that depend on both space and time. The Fourier transform of a product of functions is a convolution:

$$\int_{-\infty}^{\infty} f(x)g(x)\, e^{-ikx} dx = \frac{1}{2\pi}\left(\hat{f}\star\hat{g}\right)(k), \#(14)$$

where $\star$ is the convolution operator. The convolution can be worked out to the single integral

$$\left(\hat{f}\star\hat{g}\right)(k) = \int_{-\infty}^{\infty} f(k-\kappa)g(\kappa)\, d\kappa\,. \#(15)$$

Notice that the Fourier transform of the product results in an integration over a dummy wavenumber κ, where one function is evaluated at κ and the other is evaluated at $k-\kappa$. This integration over all wavenumbers (and later frequencies) allows different wave modes to interact nonlinearly. The Laplace transform also results in a convolution integral with the argument $\omega - \nu$, where ν is the dummy integration frequency.

At this time, we must now specify the collision operator. Physically, Coulomb collisions are an important process, however an analytic solution for the Fokker-Planck collision operator

is not supported in this framework (see *Kudeki and Milla*, 2011; *Milla and Kudeki*, 2011; and *Longley et al.*, 2019). Instead, we use the BGK operator as it has the advantage of being linear, and it adequately describes electron-neutral collisions:

$$S[t,\vec{x},\vec{v}] = -\nu_s\left(F_{1s}[t,\vec{x},\vec{v}] - \frac{n_{1s}[t,\vec{x}]}{n_{0s}}F_{0s}[\vec{v}]\right), \#(16)$$

where ν_{cs} is the collision rate, and the zeroth and first order densities relate to the distribution functions as $n_{0s} = \int d\vec{v}^3 F_{0s}[\vec{v}]$ and $n_{1s} = \int d\vec{v}^3 F_{1s}[\vec{v}]$.

The full Fourier-Laplace transform of Equation 7 is then

$$\begin{aligned}\{-i\omega - \nu_s + i(\vec{k}\cdot\vec{v})\}F_{1s}[\omega,\vec{k},\vec{v}] - F_{1s}[t_0,\vec{k},\vec{v}] + \frac{q_s}{m_s}\vec{E}_1[\omega,\vec{k}]\cdot\nabla_v F_0[\vec{v}] + \frac{q_s}{m_s}(\vec{v}\times\vec{B})\\ \cdot\nabla_v F_{1s}[\omega,\vec{k},\vec{v}]\\ = -\frac{q_s}{m_s}\frac{1}{(2\pi)^4}\int_{-\infty}^{\infty}d\vec{\kappa}^3\int_{-\infty}^{\infty}d\nu\ \vec{E}_1[\omega-\nu,\vec{k}-\vec{\kappa}]\cdot\nabla_v F_{1s}(\nu,\vec{\kappa},\vec{v})\\ + \nu_s F_{0s}[\vec{v}]n_{1s}[\omega,\vec{k}] - \frac{n_{1s}[t_0,\vec{k}]}{n_{0s}}F_{0s}[\vec{v}].\end{aligned}$$

$$\#(17)$$

2.3 Recursively Defined Equations: Breaking Self-Consistency

Thomson scatter radars such as Jicamarca work by transmitting radio pulses into the ionosphere, then measuring the weak backscattered signal. Physically, the radio waves Thomson scatter off of electrons, but a strong signal is only detected if a Bragg scattering condition is met. In a plasma, this structuring comes from waves or instability fluctuations. *Froula et al.* (2011) derives the scattering power of a collisional plasma as

$$S(\omega,\vec{k}) = 2\nu_q\left\langle\left|n_{1e}(\omega,\vec{k})\right|^2\right\rangle \#(18)$$

where ν_q is the collision frequency for electrons or ions, determined by the distribution being ensemble averaged. The quantity $S(\omega,\vec{k})$ is analogous to a scattering cross section in the radar equation:

$$P_{rec} = P_{tr}\frac{r_0^2}{2\pi A}\,S(\omega,\vec{k}). \#(19)$$

Equation 19 therefore relates P_{rec}, the power received by the radar, to constants (r_0 is the classical electron radius) and system parameters (transmitted power P_{tr} and antenna area *A*). The remaining term $S(\omega,\vec{k})$ therefore contains all the information of the plasma. Since the scattering power *S* depends directly on the electron density fluctuations n_{1e}, we can also use the following results to study density fluctuations and waves more generally.

To obtain the scattering spectra $S(\omega,\vec{k})$ in Equation 18, the perturbed electron density must be solved for and then ensemble averaged. This is done by taking a system of equations consisting of the Boltzmann equation for electrons (Equation 17), the Boltzmann equation for

ions (linearized version of Equation 17), and Gauss' law. The Fourier-Laplace transform of Gauss' law is

$$\vec{E}_1[\omega,\vec{k}] = -\frac{i}{\epsilon_0}\rho_1[\omega,\vec{k}]\frac{\vec{k}}{k^2}. \#(20)$$

The charge density therefore couples the electron and ion Boltzmann equations since $\rho_1[\omega,\vec{k}] = e\big(n_{1i}[\omega,\vec{k}] - n_{1e}[\omega,\vec{k}]\big)$.

If Gauss' law is directly substituted into Equation 17 and then integrated over velocity, the perturbed densities are

$$n_{1e}[\omega,\vec{k}] = iD_e[\omega,\vec{k}] + n_{1e}[\omega,\vec{k}]U_e[\omega,\vec{k}] + \big(n_{1i}[\omega,\vec{k}] - n_{1e}[\omega,\vec{k}]\big)H_e[\omega,\vec{k}] + \frac{1}{(2\pi)^4}\int d\vec{\kappa}^3 \int d\nu \left(n_{1i}[\omega-\nu,\vec{k}-\vec{\kappa}] - n_{1e}[\omega-\nu,\vec{k}-\vec{\kappa}]\right)\cdot G_e(\omega,\vec{k},\nu,\vec{\kappa}),$$

$$\#(21)$$

$$n_{1i}[\omega,\vec{k}] = iD_i[\omega,\vec{k}] + n_{1i}[\omega,\vec{k}]U_i[\omega,\vec{k}] - \big(n_{1i}[\omega,\vec{k}] - n_{1e}[\omega,\vec{k}]\big)H_i[\omega,\vec{k}] - \frac{1}{(2\pi)^4}\int d\vec{\kappa}^3 \int d\nu \left(n_{1i}[\omega-\nu,\vec{k}-\vec{\kappa}] - n_{1e}[\omega-\nu,\vec{k}-\vec{\kappa}]\right)\cdot G_i(\omega,\vec{k},\nu,\vec{\kappa}).$$

$$\#(22)$$

The collisional integral U_s, susceptibilities $\chi_s \equiv H_s/(1+U_S)$ and the distribution-like terms $M_s \equiv 2\nu_s\langle|D_s|\rangle$ are derived in *Froula et al.* (2011) and defined in Appendix B. The nonlinear term defines the shorthand function

$$G_s(\omega,\vec{k},\nu,\vec{\kappa}) = \frac{\omega_{ps}^2}{n_0}\int_{\vec{v}} d\vec{v}^3 \sum_{l,p}\frac{J_l(k_\perp\rho_s)J_p(k_\perp\rho_s)e^{i(m-l)\phi}}{\{\omega - k_\parallel v_\parallel - l\omega_{cs} - i\nu_s\}}\left(k_\parallel^*\frac{\partial}{\partial v_\parallel} + \frac{k_\perp^*}{k_\perp}\frac{l}{\rho_e}\frac{\partial}{\partial v_\perp}\right)f_{1s}[\nu,\vec{\kappa},\vec{v}]\,.\#$$

$$\#(23)$$

The system of Equations 21 – 22 presents a significant and insurmountable problem: the solution is a recursively defined equation. Take for example the test case where only electrons are present ($n_{1i} = 0$), Equation 21 reduces to the form

$$n_{1e}[\omega,\vec{k}]\big(1 + H_e[\omega,\vec{k}] - U_e[\omega,\vec{k}]\big) - iD_e[\omega,\vec{k}] = -\frac{1}{(2\pi)^4}\int d\vec{\kappa}^3 \int d\nu\, n_{1e}[\omega-\nu,\vec{k}-\vec{\kappa}]\cdot G_e(\omega,\vec{k},\nu,\vec{\kappa}).$$

$$\#(24)$$

On the left-hand side every function is evaluated at $(\omega,\vec{k})$, which is the desired frequency of the ion-acoustic mode with the wavenumber set by the radar's transmitted frequency. However, the right hand side involves $n_{1e}[\omega-\nu,\vec{k}-\vec{\kappa}]$, the exact quantity that is trying to be solved for at $(\omega,\vec{k})$, as well as $f_{1e}[\nu,\vec{\kappa},\vec{v}]$ (via G_e) which relates directly to $n_{1e}[\nu,\vec{k}]$. This is a recursively defined equation: the solution of $n_{1e}[\omega,\vec{k}]$ depends on $n_{1e}[\omega-\nu,\vec{k}-\vec{\kappa}]$ and $n_{1e}[\nu,\vec{k}]$. There are no standard methods for solving recursively defined equations analytically, even for the

simplest case of $f(x) + f(x - c) = a$. A numeric solution is possible through a recursive algorithm, but such a solution is very sensitive to the initial value used to start the solution.

Physically, the resulting recursive equation makes sense. To know the density fluctuations at (ω, k), one must know the fluctuations at $(\omega - \nu, k - \kappa)$ and (ν, κ). But by coupling the modes together, the density fluctuations at (ω, k) will change the fluctuations at $(\omega - \nu, k - \kappa)$, which then changes the fluctuations at (ω, k) and so on. A general solution of Equations 21 – 22 is likely impossible. However, for the case of 150-km echoes we are interested in how the high-frequency Upper-Hybrid mode affects the low-frequency ion-acoustic mode. This is fortuitous, as only electron motions are relevant for the Upper-Hybrid mode. We make the argument that the low-frequency motions from the ion-acoustic mode do not affect the high-frequency Upper-Hybrid (and Langmuir) mode at all. This argument is based on the vastly different masses of electrons and ions and is used often in plasma physics (e.g., only electrons contribute to Debye shielding).

To gain tractability, the recursively defined system of Equations 21 – 22 must be separated by time scale. The nonlinear term is assumed to only be important for high frequencies – specifically the Upper-Hybrid frequency ω_{hf}. The perturbed density and distribution in the nonlinear term are then taken to be a separate function than $n_{1s}[\omega, \vec{k}]$, and these separate functions are denoted as $n_{1s}^{hf}[\omega - \nu, \vec{k} - \vec{\kappa}]$ and $f_{1s}^{hf}[\nu, \vec{\kappa}]$. The system of equations then becomes

$$n_{1e}[\omega, \vec{k}] - iD_e[\omega, \vec{k}] - n_{1e}[\omega, \vec{k}]U_e[\omega, \vec{k}] - \left(n_{1i}[\omega, \vec{k}] - n_{1e}[\omega, \vec{k}]\right)H_e[\omega, \vec{k}] = \frac{1}{(2\pi)^4}\int d\vec{\kappa}^3 \int d\nu \left(n_{1i}^{hf}[\omega - \nu, \vec{k} - \vec{\kappa}] - n_{1e}^{hf}[\omega - \nu, \vec{k} - \vec{\kappa}]\right)G_e^{hf}(\omega, \vec{k}, \nu, \vec{\kappa}),$$

$$\#(25)$$

$$n_{1i}[\omega, \vec{k}] - iD_i[\omega, \vec{k}] - n_{1i}[\omega, \vec{k}]U_i[\omega, \vec{k}] + \left(n_{1i}[\omega, \vec{k}] - n_{1e}[\omega, \vec{k}]\right)H_i[\omega, \vec{k}] = -\frac{1}{(2\pi)^4}\int d\vec{\kappa}^3 \int d\nu \left(n_{1i}^{hf}[\omega - \nu, \vec{k} - \vec{\kappa}] - n_{1e}^{hf}[\omega - \nu, \vec{k} - \vec{\kappa}]\right)G_i^{hf}(\omega, \vec{k}, \nu, \vec{\kappa}),$$

$$\#(26)$$

where G_s^{hf} is Equation 23 evaluated with f_{1s}^{hf}. Now in Equations 25 – 26, the left-hand side is entirely functions evaluated at $(\omega, \vec{k})$, and the right-hand side is the nonlinear term with the high-frequency (*hf*) functions being effectively constants when solving for $n_{1e}[\omega, \vec{k}]$.

For the problem of 150-km echoes, photoelectron peaks will drive the Upper-Hybrid mode unstable. The first attempt at solving Equations 25 – 26 calculated the high-frequency terms (n_{1s}^{hf} and f_{1s}^{hf}) using the linear theory for Upper-Hybrid mode generation developed in *Longley et al.* (2021). This solution did not work and led to the nonlinear term being 10 orders of magnitude smaller than the linear term. This failed because the *Longley et al.* (2021) solution is linear, and therefore does not adequately describe the wave growth during an instability. The problem arises from the substitution of the perturbed electric field E_1 using Gauss' law.

Reversing the substitution of Gauss' law only for the nonlinear term, the system of equations is

$$n_{1e}[\omega,\vec{k}] - iD_e[\omega,\vec{k}] - n_{1e}[\omega,\vec{k}]U_e[\omega,\vec{k}] - \left(n_{1i}[\omega,\vec{k}] - n_{1e}[\omega,\vec{k}]\right)H_e[\omega,\vec{k}] = \frac{i\epsilon_0}{e(2\pi)^4}\int d\vec{\kappa}^3 \int d\nu\, E_1^{hf}[\omega-\nu,\vec{k}-\vec{\kappa}]\cdot G_e^{hf}(\omega,\vec{k},\nu,\vec{\kappa}),$$

#(27)

$$n_{1i}[\omega,\vec{k}] - iD_i[\omega,\vec{k}] - n_{1i}[\omega,\vec{k}]U_i[\omega,\vec{k}] + \left(n_{1i}[\omega,\vec{k}] - n_{1e}[\omega,\vec{k}]\right)H_i[\omega,\vec{k}] = -\frac{i\epsilon_0}{e(2\pi)^4}\int d\vec{\kappa}^3 \int d\nu\, E_1^{hf}[\omega-\nu,\vec{k}-\vec{\kappa}]\cdot G_i^{hf}(\omega,\vec{k},\nu,\vec{\kappa}).$$

#(28)

To solve this system of equations we will assume a value for the perturbed electric field. This is similar to how quasilinear theory requires an external evaluation of the wave amplitude (*Nicholson*, 1983). The choice of electric field value is discussed further in section 3.

Finally, we recognize that the ion distribution in G_i is evaluated at the high-frequency mode. As argued before, the high ion mass will prohibit the ions from moving at high frequencies, and therefore f_{1i}^{hf} will be zero at $\nu \approx \omega_{hf}$, effectively dropping the nonlinear term from the ion equation. Solving the system of Equations 27 – 28 with $G_i = 0$ finally yields

$$n_{1e} = \left(1-\frac{\chi_e}{\epsilon}\right)\frac{iD_e}{(1-U_e)} + \frac{\chi_e}{\epsilon}\left[\frac{iD_i}{(1-U_i)}\right] + \left(1-\frac{\chi_e}{\epsilon}\right)\frac{1}{(1-U_e)}\frac{i\epsilon_0}{e}\frac{1}{(2\pi)^4}\int d\vec{\kappa}^3 \int d\nu\, E_1^{hf}[\omega-\nu,\vec{k}-\vec{\kappa}]G_e^{hf}(\omega,\vec{k},\nu,\vec{\kappa}).$$

#(29)

2.4 Solving for the Scattering Spectra

To obtain the scattering spectra, Equation 29 is squared and ensemble averaged:

$$\langle|n_{1e}|^2\rangle = \left|1-\frac{\chi_e}{\epsilon}\right|^2\frac{M_e}{2\nu_e} + \left|\frac{\chi_e}{\epsilon}\right|^2\frac{M_i}{2\nu_i} + \left|1-\frac{\chi_e}{\epsilon}\right|^2\frac{1}{|1-U_e|^2}\frac{\epsilon_0^2}{e^2}\frac{1}{(2\pi)^8} \cdot \left\langle \int d\vec{\kappa_1}^3 \int d\nu_1\, E_1^{hf}[\omega-\nu_1,\vec{k}-\vec{\kappa}_1]\cdot G_e^{hf}(\omega,\vec{k},\nu_1,\vec{\kappa}_1) \cdot CC\left\{\int d\vec{\kappa_2}^3 \int d\nu_2\, E_1^{hf}[\omega-\nu_2,\vec{k}-\vec{\kappa}_2]\cdot G_e^{hf}(\omega,\vec{k},\nu_2,\vec{\kappa}_2)\right\}\right\rangle,$$

#(30)

where *CC* denotes a complex conjugate, and the angle brackets denote the ensemble average defined in *Froula et al.* (2011):

$$\langle X\rangle = \frac{\int d\nu\, X(\nu)\, P(\nu)}{\int d\nu\, P(\nu)}. \#(31)$$

$P(\nu)$ is the probability of finding the system in state *v*, and there is a velocity coordinate in the integral for each particle in the system (i.e., $\int d\nu_1\, d\nu_2 \ldots d\nu_N$).

In Equation 30, the first two terms define the scattering spectra from linear theory (*Froula et al.*, 2011; *Kudeki and Milla*, 2011). The functions M_s are defined in Appendix B, and physically represent the scattering from a non-interacting gas of particles. The factor χ_e/ϵ is very large at normal wave modes where $\epsilon \to 0$, and shows how the scattering spectra (and density fluctuations) are strongest when waves are present to create the structuring for Bragg scattering.

The remaining nonlinear term in Equation 30 shows that the mode coupling is an additive term to the density fluctuations and can be evaluated independently from the linear terms. The challenge of the nonlinear term is its integration over all frequency and wavenumber space. First, we will simplify the number of integrals by assuming a spherical symmetry to the system, so the wavenumber integrations simplify as

$$\int d\vec{\kappa}^3 F = 4\pi \int_0^\infty d\kappa\, \kappa^2\, F\,. \#(32)$$

The frequency integration is approximated by assuming the integrand is shaped as a Lorentzian over frequency. This is partially justified in *Longley et al.* (2021), which showed that a Lorentzian describes the frequency dependence of density fluctuations of the Upper-Hybrid mode.

$$\int_{-\infty}^{\infty} d\nu\, F = 2\gamma\left[\omega_{hf}, \vec{k}_{hf}\right] F. \#(33)$$

Effectively, the growth/damping rate γ of the Upper-Hybrid mode determines the width of the Lorentzian. Setting $\nu = \omega_{hf}$ as the center frequency of the Upper-Hybrid mode also sets $\vec{\kappa} = \vec{k}_{hf}$ through solving the dispersion relation $\mathrm{Re}\left[\epsilon\left(\omega_{hf}, \vec{k}_{hf}\right)\right] = 0$.

Putting Equations 32 and 33 into Equation 30, with $\kappa \to k_{hf}$:

$$\begin{aligned}\langle |n_{1e}|^2 \rangle = {} & \left|1 - \frac{\chi_e}{\epsilon}\right|^2 \frac{M_e}{2\nu_e} + \left|\frac{\chi_e}{\epsilon}\right|^2 \frac{M_i}{2\nu_i} + \left|1 - \frac{\chi_e}{\epsilon}\right|^2 \frac{1}{|1 - U_e|^2} \frac{\epsilon_0^2}{e^2} \frac{4\pi \cdot 4\pi}{(2\pi)^8} \\ & \cdot \left\langle \int dk_{hf,1}\, k_{hf,1}^2 2\gamma\left[\omega_{hf}, k_{hf,1}\right] E_1\left[\omega - \omega_{hf,1}, \vec{k} - \vec{k}_{hf,1}\right] \cdot G_e\left(\omega, \vec{k}, \omega_{hf,1}, \vec{k}_{hf,1}\right) \right. \\ & \cdot CC \left\{ \int dk_{hf,2}\, k_{hf,2}^2 2\gamma\left[\omega_{hf}, k_{hf,2}\right] E_1\left[\omega - \omega_{hf,2}, \vec{k} - \vec{k}_{hf,2}\right] \right. \\ & \left. \left. \cdot G_e\left(\omega, \vec{k}, \omega_{hf,2}, \vec{k}_{hf,2}\right) \right\} \right\rangle. \end{aligned}$$

$$\#(34)$$

The result involves the multiplication of two single variable integrals. While this double integral follows from squaring the nonlinear term, it lacks an obvious physical meaning. The derivation in this paper makes several approximations that are weakly justified, with the goal of obtaining an analytic solution. As written, Equation (34) is intractable unless the unjustified approximation of $k_{hf,1} = k_{hf,2}$ is made. In this step, the integration over k_{hf} is also discretized, and therefore taking $k_{hf,1} = k_{hf,2}$ is equivalent to taking the diagonal terms in the product of summations:

$$\langle |n_{1e}|^2 \rangle = \left|1 - \frac{\chi_e}{\epsilon}\right|^2 \frac{M_e}{2\nu_e} + \left|\frac{\chi_e}{\epsilon}\right|^2 \frac{M_i}{2\nu_i} + \left|1 - \frac{\chi_e}{\epsilon}\right|^2 \frac{1}{|1-U_e|^2} \frac{\epsilon_0^2}{4\pi^6 e^2} \gamma^2\left[\omega_{hf}, k_{hf}\right] \cdot \left\langle \sum_{all\ k_{hf}} \Delta k_{hf}^2 k_{hf}^4 \left|\vec{E}_1\left[\omega - \omega_{hf}, \vec{k} - k_{hf}\right] \cdot \vec{\mathcal{G}}_e\left(\omega, \vec{k}, \omega_{hf}, \vec{k}_{hf}\right)\right|^2 \right\rangle. \quad \#(35)$$

The electric field will be externally imposed, and therefore does not depend on the ensemble average and is factored out. Substituting back for G_e yields

$$\langle |n_{1e}|^2 \rangle = \left|1 - \frac{\chi_e}{\epsilon}\right|^2 \frac{M_e}{2\nu_e} + \left|\frac{\chi_e}{\epsilon}\right|^2 \frac{M_i}{2\nu_i} + \left|1 - \frac{\chi_e}{\epsilon}\right|^2 \frac{1}{|1-U_e|^2} \frac{\epsilon_0^2}{4\pi^6 e^2} \frac{\omega_{pe}^4}{n_0^2 k^{*2}} \gamma^2\left[\omega_{hf}, k_{hf}\right] \cdot \sum_{all\ k_{hf}} \Delta k_{hf}^2 k_{hf}^4 \left|E_1\left[\omega^*, \vec{k}^*\right]\right|^2 \left\langle \left| \int_{\vec{v}} d\vec{v}^3 \sum_{l,p} \frac{J_l(k_\perp \rho_e) J_p(k_\perp \rho_e) e^{i(m-l)\phi}}{\{\omega - k_\parallel v_\parallel - l\omega_{ce} - i\nu_e\}} \cdot \left(k_\parallel^* \frac{\partial}{\partial v_\parallel} + \frac{k_\perp^*}{k_\perp} \frac{l}{\rho_e} \frac{\partial}{\partial v_\perp} \right) f_{1e}^{hf}\left[\omega_{hf}, \vec{k}_{hf}, \vec{v}\right] \right|^2 \right\rangle, \quad \#(36)$$

where we define the shifted frequencies and wavenumbers as

$$\omega^* = \omega - \omega_{hf}, \#(37)$$

$$\vec{k}^* = \vec{k} - \vec{k}_{hf}. \#(38)$$

with $\left(\omega, \vec{k}\right)$ being low-frequency values.

2.5 Summary of Solution

Equation 36 is the final solution for the electron density fluctuations at low frequencies. It includes contributions from all possible driving wavenumbers, k_{hf}. Since the integration over k_{hf} was discretized, we can either search for the contributions from a single driving source or add up the contributions from multiple sources to obtain a realistic result of the Upper-Hybrid mode being excited across a wide range of wavenumbers.

To obtain the scattering power, Equation 18 is combined with Equation 36:

$$S\left(\omega, \vec{k}\right) = \left|1 - \frac{\chi_e}{\epsilon}\right|^2 M_e + \left|\frac{\chi_e}{\epsilon}\right|^2 M_i + \sum_{all\ k_{hf}} \nu_e \left|1 - \frac{\chi_e}{\epsilon}\right|^2 \frac{1}{|1-U_e|^2} \frac{\epsilon_0^2 \gamma^2\left[\omega_{hf}, k_{hf}\right] \Delta k_{hf}^2}{2\pi^6 e^2} \frac{\omega_{pe}^4 k_{hf}^4}{n_0^2 k^{*2}} \cdot \left|E_1\left[\omega^*, \vec{k}^*\right]\right|^2 \cdot \langle T \rangle. \quad \#(39)$$

The ensemble average term in Equation 39 is defined as

$$\langle T\rangle \equiv \frac{1}{N}\left\langle \left| \int_{\vec{v}} d\vec{v}^3 \sum_{l,p} \frac{J_l(k_\perp \rho_e) J_p(k_\perp \rho_e) e^{i(m-l)\phi}}{\{\omega - k_\parallel v_\parallel - l\omega_{ce} - i\nu_e\}} \cdot \left(k_\parallel^* \frac{\partial}{\partial v_\parallel} + \frac{k_\perp^*}{k_\perp} \frac{l}{\rho_e} \frac{\partial}{\partial v_\perp} \right) f_{1s}^{hf}\left[\omega_{hf}, \vec{k}_{hf}, \vec{v}\right] \right|^2 \right\rangle$$

#(40)

The remaining task is to evaluate Equation 40. Note that in Equation 40 there are three different frequency/wavenumber combinations: the low frequency mode $(\omega, \vec{k})$ that came from solving for the density fluctuations; the shifted wavenumber $\vec{k}^*$ that came from the direction of $\vec{E}_1(\omega^*, \vec{k}^*)$, and the high frequency mode $(\omega_{hf}, \vec{k}_{hf})$ at which the perturbed distribution is evaluated. Since $f_{1s}^{hf}\left[\omega_{hf}, \vec{k}_{hf}, \vec{v}\right]$ is evaluated at high frequencies and driven by photoelectrons, the linear theory from *Longley et al.* (2021) is appropriate for calculating f_{1s}^{hf} as the high frequency response of electrons to perturbations. This term from *Longley et al.* (2021) is then

$$\begin{aligned} f_{1e}^{hf}\left(\omega_{hf}, \vec{k}_{hf}, \vec{v}\right) &= \left(\frac{D_1^{hf}}{1 + H_1^{hf}}\right) \cdot \sum_{l,p} \frac{J_l(k_\perp \rho_s) J_p(k_\perp \rho_s) e^{i(l-p)\phi}}{\left\{\omega_{hf} - k_{hf,\parallel} v_\parallel - l\omega_{ce} - i\nu_e\right\}} \left[\frac{\omega_{pe}^2}{n_0 k_{hf}^2} \vec{k}_{hf} \cdot \frac{\partial F_{0e}}{\partial \vec{v}^*} + i\nu_e f_{0e} \right] \\ &\quad - \sum_{l,p} \frac{J_l(k_\perp \rho_s) J_p(k_\perp \rho_s) e^{i(l-p)\phi}}{\left\{\omega_{hf} - k_{hf,\parallel} v_\parallel - l\omega_{ce} - i\nu_e\right\}} \left[i f_{1e}\left[t_0, \vec{k}_{hf}, \vec{v}\right] - i n_{1e}\left[t_0, \vec{k}_{hf}\right] f_{0e} \right], \end{aligned}$$

#(41)

where the functions in the leading factor are

$$H_1^{hf} = \int d\vec{v} \left\{ \sum_{l,p} \frac{J_l(k_\perp \rho_s) J_p(k_\perp \rho_s) e^{i(l-p)\phi}}{\left\{\omega_{hf} - k_{hf,\parallel} v_\parallel - l\omega_{ce} - i\nu_e\right\}} \left[\frac{\omega_{pe}^2}{n_0 k_{hf}^2} \vec{k}_{hf} \cdot \frac{\partial F_{0e}}{\partial \vec{v}^*} + i\nu_e f_{0e} \right] \right\}, \#(42)$$

$$D_1^{hf} = \int d\vec{v} \left\{ \sum_{l,p} \frac{J_l(k_\perp \rho_s) J_p(k_\perp \rho_s) e^{i(l-p)\phi}}{\left\{\omega_{hf} - k_{hf,\parallel} v_\parallel - l\omega_{ce} - i\nu_e\right\}} \left[i f_{1e}\left[t_0, \vec{k}_{hf}, \vec{v}\right] - i n_{1e}\left[t_0, \vec{k}_{hf}\right] f_{0e} \right] \right\}. \#(43)$$

The results contain velocity integrations over multiple poles that must be dealt with. For example, the first term in the expanded ensemble average is

$$\langle T\rangle_{a,1} = \frac{4\pi k_{\parallel}^{*2} \nu_e}{k_{hf,\parallel}^2 k_{\parallel}^2} \sum_{x,n} \int_0^\infty dv_\perp v_\perp J_x^2\left(k_{hf,\perp}\rho_e\right) J_n^2(k_\perp \rho_e) \cdot \int_{-\infty}^{\infty} dv_\parallel \left(\frac{f_0(v_\perp, v_\parallel)}{\left\{v_\parallel - \frac{\omega - x\Omega_{ce} - i\nu_e}{k_{hf,\parallel}}\right\}\left\{v_\parallel - \frac{\omega - x\Omega_{ce} + i\nu_e}{k_{hf,\parallel}}\right\}} \cdot \frac{1}{\left\{v_\parallel - \frac{\omega - n\Omega_{ce} - i\nu_e}{k_\parallel}\right\}^2 \left\{v_\parallel - \frac{\omega - n\Omega_{ce} + i\nu_e}{k_\parallel}\right\}^2} \right).$$

#(44)

Typically, linear solutions will only result in one or two simple poles in the denominator, and therefore the Plemelj theorem can be applied as an analytic solution for the $v_\parallel$ integral. However, the Plemelj theorem results in principal value integrals that are not easy for either non-Maxwellian distributions or multiple poles. For this reason, the integrations are evaluated numerically over $v_\parallel$ and $v_\perp$ (the integration over ϕ is already performed, resulting in a factor of 2π due to cylindrical symmetry). The poles lead to difficulties in the $v_\parallel$ integration, though working in the collisional regime means the pole is displaced away from the real axis. An algorithm was constructed to evaluate the $v_\parallel$ integrals along the real line by choosing a velocity mesh with high resolution centered at each pole.

At this point, the physical derivation is complete. The mathematical solution for Equations 40 – 41 is lengthy but straight forward, so the results are listed in Appendix A. Readers interested in a step-by-step calculation of these terms can consult the materials in the "Open Research" statement of this manuscript, which also includes the code used to calculate spectra from equation 39.

3 Application to 150-km Echoes

The nonlinear mode coupling developed in Section 2 applies to any set of waves that are substantially separated in frequency, meaning $\omega \ll \omega_{hf}$. This mode coupling framework explains how the photoelectron driven instability in *Longley et al.* (2020, 2021) can generate 150-km echoes. The generation mechanism is as follows:

1. Peaks are created in the photoelectron distribution. A collisional resonance with N^2 creates a dip at ~2.5 eV that manifests as a peak at ~5 eV. Additionally, EUV emission lines from the Sun create peaks in the range of 10-30 eV. See *Oppenheim and Dimant* (2016) and *Chau et al.* (2023).
2. The photoelectron peaks drive a bump-on-tail like instability. This instability excites the Langmuir/Upper-Hybrid mode at high frequencies ($\omega_{hf} \approx \omega_{pe}$, typically 5-10 MHz) and short wavelengths (~20 cm). The linear theory of this instability is derived in *Longley et al.* (2020, 2021).

3. At high enough wave amplitudes, the unstable Upper-Hybrid mode couples nonlinearly to the low frequency ion-acoustic mode ($\omega \approx \omega_{ia}$, typically ~kHz) through the mechanism derived in Section 2.

Observationally, 150-km echoes are a 10-20 dB enhancement of the ion-acoustic mode. They are observed where photoelectron production is the highest (130-180 km), and only in directions nearly perpendicular to Earth's magnetic field. To calculate the scattering spectra in Equation 39, we specify the zeroth order distribution as the summation of a thermal Maxwellian population, and a photoelectron population with a power-law tail and bump-on-tail features at V_i = 5, 15, 25, and 45 eV. This is the same photoelectron distribution used in *Longley et al.* (2021) and is advantageous as it allows derivatives to be calculated analytically.

The theory in Section 2 requires the electric field amplitude of the high-frequency mode $E_1[\omega^*, \vec{k}^*]$ to be specified externally. Determining the saturated amplitude of an instability is an open problem in plasma physics. Therefore, this remains a free parameter in the calculation. In *Derghazarian et al.* (2023) a similar problem of cross-wavelength coupling between lower-hybrid waves was studied. In that study, a range of wave amplitudes from 20 μV/m to 20 mV/m is used based on in situ measurements. Since the scattering power in Section 2 varies as $S \propto |E_1|^2$, we do not need to investigate a range of wave amplitudes as each order of magnitude increase results in a 20 dB power increase. We make the choice of using a 1 μV/m electric field, as it is an order of magnitude estimate well below the wave amplitudes studied in *Derghazarian et al.* (2023), and it produces realistic results.

Figure 2 shows the calculated ion-acoustic mode spectra for a single driving wavenumber of $k_{hf} = 24$, adding the contributions of both the upshifted (positive k_{hf}, wave traveling to radar) and downshifted (negative k_{hf}) Upper-Hybrid mode. The enhancement of the nonlinear spectra (S_{NL}) is calculated in dB as

$$dB = 10 \log\left(\frac{\max(S_{NL})}{\max(S_{linear})}\right), \#(45)$$

where the linear spectra are calculated from *Kudeki and Milla* (2011). In several panels of Figure 2, a noticeable left-right asymmetry is present in the nonlinear spectra. Mathematically, this results from the dependence on the resonant velocities $y_n^{lf} = (\omega - n\Omega_{ce} - i\nu_e)/k_\parallel$. Physically, this could be a preferential coupling between wave modes traveling in one direction versus another, but a full explanation of this asymmetry is currently not available. Nonetheless, Figure 7 in *Chau et al*. (2023) shows an asymmetry is present in the data.

The results in Figure 2 show that the level of the enhancement depends strongly on the radar wavenumber and the plasma density. The sensitivity to plasma density, through the ratio $\omega_{UH}/\Omega_{ce} = \sqrt{\omega_{pe}^2 + \Omega_{ce}^2}/\Omega_{ce}$, is expected as *Lehmacher et al.* (2020) showed experimentally that forbidden gaps in 150-km echoes occur when ω_{UH}/Ω_{ce} is an integer. Analytic work in *Longley et al.* (2020) showed this same condition leads to the suppression of the instability by thermal Landau damping.

Observationally, 150-km echoes have only been observed by radars with transmit frequencies in the range of 30-50 MHz (*Kudeki and Fawcett*, 1993; *Patra et al*., 2020a). Notably, the ALTAIR radar (150 MHz) has never observed 150-km echoes despite its favorable location at the equator (*Chau et al*, 2023). In Figure 2, the enhancement is weakest at 150 MHz, but still

present for the $\omega_{UH}/\Omega_{ce} = 3.84$ condition. Equation 39 shows the imposed wave electric field is a function of radar wavenumber, $E_1[\omega^*, \vec{k}^*]$, but the results in Figure 2 use the same E_1 for each $k^* \equiv k - k_{hf}$ value. At higher radar wavenumbers, $E_1[\omega^*, \vec{k}^*]$ is evaluated further away from the dispersion relation at (ω_{hf}, k_{hf}), and therefore the driving electric field for a 150 MHz radar should be smaller than the driving electric field for 30-50 MHz radars. This means that ALTAIR has not observed 150-km echoes due to its frequency being too high, which inhibits the wave coupling and leads to lower $E_1[\omega^*, \vec{k}^*]$ values evaluated away from the dispersion relation.

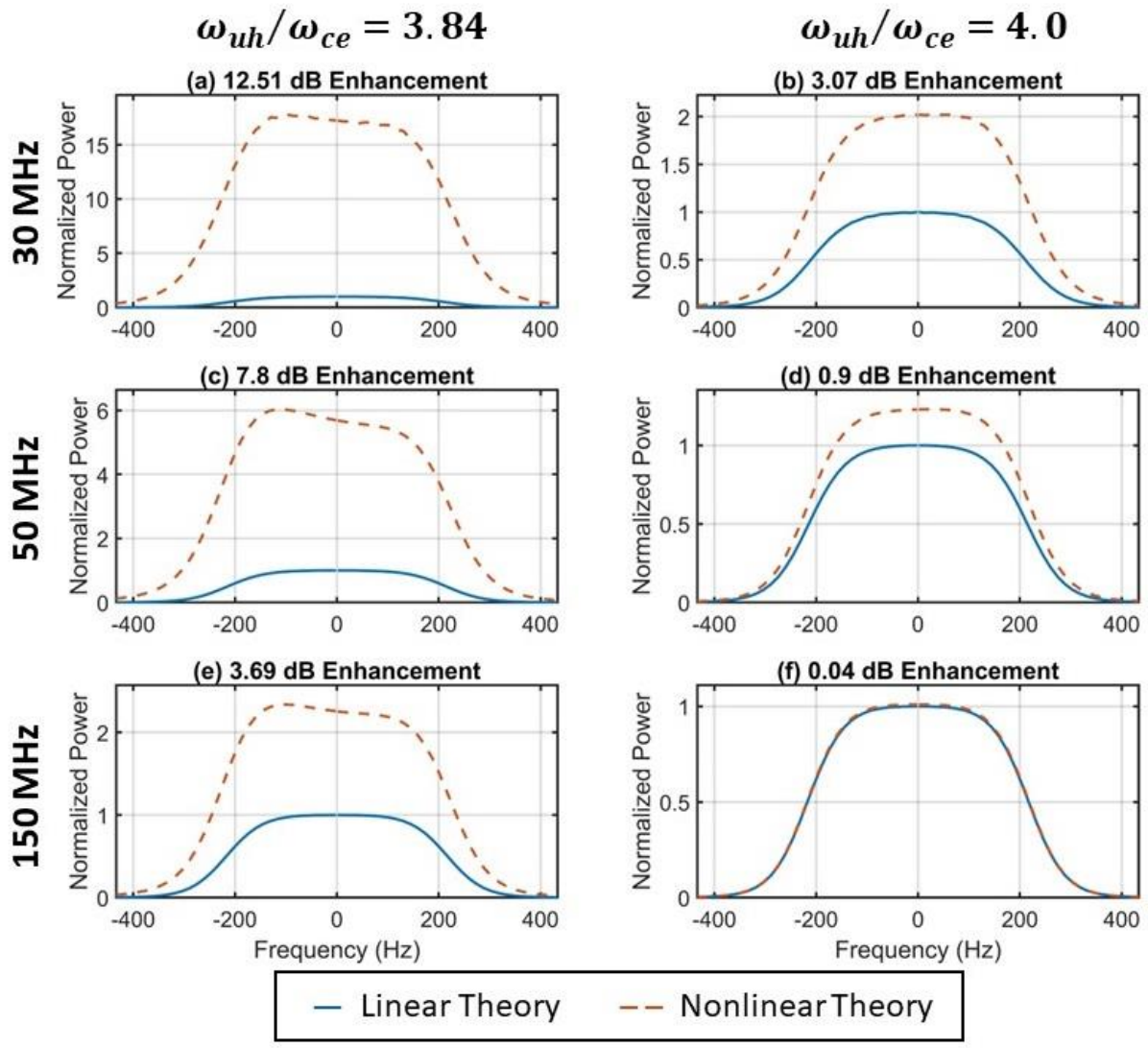

Figure 2. Calculated ion-acoustic mode spectra, for different radars and plasma densities. Panels (a) – (b) show the results for a 30 MHz radar (5-meter Bragg wavelength, $k = 1.26$), panels (c) – (d) show the results for a 50 MHz radar (3-meter wavelength, $k = 2.1$), and panels (e) – (f) are for a 150 MHz radar (1-meter wavelength, $k = 6.3$). The density is chosen such that $\omega_{UH} = 3.84\Omega_{ce}$ in panels (a), (c), and (e), and $\omega_{UH} = 4.0\Omega_{ce}$ in panels (b), (d), and (f). In each panel, the spectra are normalized to the maximum value of the linear theory (solid blue curve).

4 Summary

The generation mechanism of 150-km echoes is now a solved problem. The nonlinear theory developed in this paper bridges the gap between decades of observations and the linear instability work in *Longley et al.* (2020; 2021). As discussed in the review paper *Chau et al.* (2023), there are numerous outstanding questions with 150-km echoes which this paper cannot explain. However, understanding the generation mechanism is the first step to understanding more complex details in the echoes. Furthermore, this work only explains the more common but weaker type of echo termed naturally enhanced incoherent scatter (NEIS) and does not apply to the stronger but less common field aligned irregularities (FAI), though the two types are often observed simultaneously (*Chau and Kudeki*, 2013; *Patra et al.*, 2020b). Clearly, more work is needed to fully understand 150-km echoes and their unique combination of plasma dynamics, neutral dynamics, and photochemistry.

The nonlinear mode coupling described in this paper works for any set of electrostatic waves with a separation of frequencies. The use of a driving wave electric field means this theory can be applied to HF heating problems with minimal modifications. In *Derghazarian et al.* (2021; 2023) high altitude (~2000 km) echoes are observed by Jicamarca with strong enhancements in the lower-hybrid mode. An initial search was done to see if the lower-hybrid mode is excited by the photoelectron instability, but no such enhancements were found.

The use of an externally determined wave electric field was necessary but leaves an open question of what value should be used. The theory in this paper could be fit to the observed power in 150-km echoes, giving an experimental estimate of what the wave amplitude should be. Additionally, the method in this paper of breaking the self-consistency of the nonlinear term can be applied to the photoelectron instability theory, possibly determining the wave amplitude from theory. Both approaches would lead to new insights into how instabilities reach a saturated state.

Appendix A: Results of Nonlinear Theory

The nonlinear term in Equation 39 is

$$S_{NL}(\omega, \vec{k}) = \nu_e \left|1 - \frac{\chi_e}{\epsilon}\right|^2 \frac{1}{|1 - U_e|^2} \frac{\epsilon_0^2 \gamma^2 [\omega_{hf}, k_{hf}] \Delta k_{hf}^2}{2\pi^6 e^2} \frac{\omega_{pe}^4 k_{hf}^4}{n_0^2 k^{*2}} \cdot \left|E_1[\omega^*, \vec{k}^*]\right|^2 \cdot \langle T \rangle . \#(A1)$$

The leading factors are all constants or obtained from linear theory (*Froula et al.*, 2011). The term $\langle T \rangle$ captures all the nonlinear mode coupling and is broken into many different terms based on the poles of each integral:

$$\langle T \rangle = \langle T \rangle_a + \langle T \rangle_b + \langle T \rangle_c + \langle T \rangle_d + \langle T \rangle_e + \langle T \rangle_f . \#(A2)$$

Each of these terms is integrated numerically using the distribution function from *Longley et al.* (2021). The results also use the following definitions of resonant velocities:

$$y_x^{hf} = \frac{\omega - x\Omega_{ce} - i\nu_e}{k_{hf,\parallel}}, \#(A3)$$

$$y_n^{lf} = \frac{\omega - n\Omega_{ce} - i\nu_e}{k_\parallel}. \#(A4)$$

An overbar is used to denote complex conjugate.

The first term is subdivided as

$$\langle T\rangle_a = \langle T\rangle_{a,1} + \langle T\rangle_{a,2.1} + \langle T\rangle_{a,2.2} + \langle T\rangle_{a,2.3} + \langle T\rangle_{a,3.1} + \langle T\rangle_{a,3.2} + \langle T\rangle_{a,3.3}. \#(A5)$$

and the results are

$$\langle T\rangle_{a,1} = \frac{4\pi k_\parallel^{*2}\nu_e}{k_{hf,\parallel}^2 k_\parallel^2} \sum_{x,n} \int dv_\perp v_\perp J_x^2\left(k_{hf,\perp}\rho_e\right) J_n^2(k_\perp\rho_e) \cdot \int dv_\parallel \frac{f_0(v_\perp, v_\parallel)}{\left\{v_\parallel - y_x^{hf}\right\}\left\{v_\parallel - \overline{y_x^{hf}}\right\}\left\{v_\parallel - y_n^{lf}\right\}^2\left\{v_\parallel - \overline{y_n^{lf}}\right\}^2}, \#(A6)$$

$$\langle T\rangle_{a,2.1} = -\frac{4\pi k_\perp^* k_\parallel^* \nu_e}{k_{hf,\parallel}^2 k_\parallel^2} \mathrm{Re}\left[\sum_{x,n} n \int dv_\perp J_x^2\left(k_{hf,\perp}\rho_e\right) J_n(k_\perp\rho_e)\left(J_{n-1}(k_\perp\rho_e) - J_{n+1}(k_\perp\rho_e)\right) \cdot \int dv_\parallel \frac{f_0(v_\perp, v_\parallel)}{\left\{v_\parallel - y_x^{hf}\right\}\left\{v_\parallel - \overline{y_{x'}^{hf}}\right\}\left\{v_\parallel - y_n^{lf}\right\}\left\{v_\parallel - \overline{y_n^{lf}}\right\}^2}\right], \#(A7)$$

$$\langle T\rangle_{a,2.2} = -\frac{4\pi k_\perp^* k_\parallel^* \nu_e}{k_{hf,\parallel}^2 k_\parallel^2} \mathrm{Re}\left[\sum_{x,n} n \int dv_\perp J_x^2\left(k_{hf,\perp}\rho_e\right) J_n(k_\perp\rho_e) J_{n-1}(k_\perp\rho_e) \cdot \int dv_\parallel \frac{f_0(v_\perp, v_\parallel)}{\left\{v_\parallel - y_x^{hf}\right\}\left\{v_\parallel - \overline{y_{x'}^{hf}}\right\}\left\{v_\parallel - y_n^{lf}\right\}\left\{v_\parallel - \overline{y_{n-1}^{lf}}\right\}^2}\right], \#(A8)$$

$$\langle T\rangle_{a,2.3} = \frac{4\pi k_\perp^* k_\parallel^* \nu_e}{k_{hf,\parallel}^2 k_\parallel^2} \mathrm{Re}\left[\sum_{x,n} (n-1) \int dv_\perp J_x^2\left(k_{hf,\perp}\rho_e\right) J_n(k_\perp\rho_e) J_{n-1}(k_\perp\rho_e) \cdot \int dv_\parallel \frac{f_0(v_\perp, v_\parallel)}{\left\{v_\parallel - y_x^{hf}\right\}\left\{v_\parallel - \overline{y_{x'}^{hf}}\right\}\left\{v_\parallel - \overline{y_{n-1}^{lf}}\right\}\left\{v_\parallel - y_n^{lf}\right\}^2}\right],$$

$$\#(A9)$$

$$\langle T\rangle_{a,3.1} = \frac{\pi k_\perp^{*\,2}\nu_e}{k_{hf,\parallel}^2 k_\parallel^2}\sum_{x,n} n^2 \int \frac{dv_\perp}{v_\perp} J_x^2\left(k_{hf,\perp}\rho_e\right)\left[\left(J_{n-1}(k_\perp\rho_e) - J_{n+1}(k_\perp\rho_e)\right)^2 + 2J_n^2(k_\perp\rho_e)\right] \cdot \int dv_\parallel \frac{f_0(v_\perp, v_\parallel)}{\left\{v_\parallel - y_x^{hf}\right\}\left\{v_\parallel - \overline{y_x^{hf}}\right\}\left\{v_\parallel - y_n^{lf}\right\}\left\{v_\parallel - \overline{y_n^{lf}}\right\}},$$

$$\#(A10)$$

$$\langle T\rangle_{a,3.2} = \frac{2\pi k_\perp^{*\,2}\nu_e}{k_{hf,\parallel}^2 k_\parallel^2}\sum_{x,n} n(n+1) \cdot \mathrm{Re}\left[\int \frac{dv_\perp}{v_\perp} J_x^2\left(k_{hf,\perp}\rho_e\right)\left[\left(J_{n-1}(k_\perp\rho_e) - J_{n+1}(k_\perp\rho_e)\right)J_{n+1}(k_\perp\rho_e) - J_n(k_\perp\rho_e)\left(J_n(k_\perp\rho_e) - J_{n+2}(k_\perp\rho_e)\right)\right] \cdot \int dv_\parallel \frac{f_0(v_\perp, v_\parallel)}{\left\{v_\parallel - y_x^{hf}\right\}\left\{v_\parallel - \overline{y_x^{hf}}\right\}\left\{v_\parallel - y_n^{lf}\right\}\left\{v_\parallel - \overline{y_{n+1}^{lf}}\right\}}\right],$$

$$\#(A11)$$

$$\langle T\rangle_{a,3.3} = -\frac{2\pi k_\perp^{*\,2}\nu_e}{k_{hf,\parallel}^2 k_\parallel^2}\sum_{x,n} n(n+2) \cdot \mathrm{Re}\left[\int \frac{dv_\perp}{v_\perp} J_x^2\left(k_{hf,\perp}\rho_e\right)J_n(k_\perp\rho_e)J_{n+2}(k_\perp\rho_e) \cdot \int dv_\parallel \frac{f_0(v_\perp, v_\parallel)}{\left\{v_\parallel - y_x^{hf}\right\}\left\{v_\parallel - \overline{y_x^{hf}}\right\}\left\{v_\parallel - y_n^{lf}\right\}\left\{v_\parallel - \overline{y_{n+2}^{lf}}\right\}}\right].$$

$$\#(A12)$$

The next term $\langle T\rangle_b$ is broken up as $\langle T\rangle_b = \langle T\rangle_{b,\parallel} + \langle T\rangle_{b,\perp}$, with

$$\langle T\rangle_{b,\parallel} = \frac{8\pi k_\parallel^* \nu_e}{k_{hf,\parallel}^2 k_\parallel}\mathrm{Re}\left[Y_{H1}^{hf}\sum_{x,n}\int dv_\perp\, v_\perp J_x^2\left(k_{hf,\perp}\rho_e\right)J_n^2(k_\perp\rho_e) \cdot \int dv_\parallel \frac{f_0(v_\perp, v_\parallel)}{\left\{v_\parallel - y_x^{hf}\right\}\left\{v_\parallel - \overline{y_x^{hf}}\right\}\left\{v_\parallel - \overline{y_n^{lf}}\right\}^2}\right],$$

$$\#(A13)$$

$$\langle T\rangle_{b,\perp} = -\frac{4\pi k_\perp^* \nu_e}{k_{hf,\parallel}^2 k_\parallel}\mathrm{Re}\left[Y_{H1}^{hf}\sum_{x,n} n\int dv_\perp\, J_x^2\left(k_{hf,\perp}\rho_e\right)B\left(k_\perp,\underline{n},n\right)\right.$$
$$\left.\cdot\int dv_\parallel\,\frac{f_0(v_\perp,v_\parallel)}{\left\{v_\parallel - y_x^{hf}\right\}\left\{v_\parallel-\overline{y_x^{hf}}\right\}\left\{v_\parallel-\overline{y_n^{lf}}\right\}}\right], \#(A14)$$

where Equation A14 uses the product of Bessel functions:

$$B\left(k_\perp,\underline{n},n\right) = 2J_n(k_\perp\rho_e)\left(J_{n-1}(k_\perp\rho_e) - J_{n+1}(k_\perp\rho_e)\right). \#(A15)$$

The next term is

$$\langle T\rangle_c = \frac{4\pi\nu_e}{k_{hf,\parallel}^2}\left|Y_{H1}^{hf}\right|^2\sum_x\int dv_\perp\, v_\perp\, J_x^2\left(k_{hf,\perp}\rho_e\right)\cdot\int dv_\parallel\frac{f_0(v_\perp,v_\parallel)}{\left\{v_\parallel-y_x^{hf}\right\}\left\{v_\parallel-\overline{y_x^{hf}}\right\}}. \#(A16)$$

The $\langle T\rangle_d$ term is broken up as $\langle T\rangle_d = \langle T\rangle_d^\parallel + \langle T\rangle_d^\perp$:

$$\langle T\rangle_{d,\parallel} = \frac{8\pi k_\parallel^*\nu_e}{k_{hf,\parallel}k_\parallel}\mathrm{Re}\left[\left(iZ^{hf} - \frac{i}{\nu_e}Y_{H1}^{hf}U_e^{hf}\right)\right.$$
$$\cdot\sum_{x,n}\int dv_\perp\, v_\perp\, J_{x+n}\left(\left(k_{hf,\perp}+k_\perp\right)\rho_e\right)J_x\left(k_{hf,\perp}\rho_e\right)J_n(k_\perp\rho_e)$$
$$\left.\cdot\int_{-\infty}^{\infty}dv_\parallel\,\frac{f_0(v_\perp,v_\parallel)}{\left\{v_\parallel-\overline{y_x^{hf}}\right\}\left\{v_\parallel-\overline{y_n^{lf}}\right\}^2}\right], \#(A17)$$

$$\langle T\rangle_{d,\perp} = \frac{4\pi k_\perp^*\nu_e}{k_{hf,\parallel}k_\parallel}\mathrm{Re}\left[\left(i\overline{Z^{hf}} - \frac{i}{\nu_e}\overline{Y_{H1}^{hf}}\,\overline{U_e^{hf}}\right)\right.$$
$$\left.\cdot\sum_{x,n} n\int dv_\perp B^D\left(k_{hf,\perp},k_\perp,x,n\right)\cdot\int_{-\infty}^{\infty}dv_\parallel\frac{f_0(v_\perp,v_\parallel)}{\left\{v_\parallel-y_x^{hf}\right\}\left\{v_\parallel-y_n^{lf}\right\}}\right]. \#(A18)$$

The last two terms are straightforward:

$$\langle T\rangle_e = \frac{8\pi\nu_e}{k_{hf,\parallel}}\mathrm{Re}\left[i\left(Z^{hf}\overline{Y_{H1}^{hf}} - \frac{1}{\nu_e}\left|Y_{H1}^{hf}\right|^2U_e^{hf}\right)\cdot\sum_x\int dv_\perp\, v_\perp\, J_x^2\left(k_{hf,\perp}\rho_e\right)\int_{-\infty}^{\infty}dv_\parallel\frac{f_0(v_\perp,v_\parallel)}{\left\{v_\parallel-\overline{y_x^{hf}}\right\}}\right], \#(A19)$$

$$\langle T\rangle_f = 2\left(Z^{hf}\overline{Y_{H1}^{hf}}\,\overline{U_e^{hf}} + \overline{Z^{hf}}Y_{H1}^{hf}U_e^{hf}\right) + 2\nu_e\left|Z^{hf}\right|^2 + \frac{2}{\nu_e}\left|Y_{H1}^{hf}\right|^2\left|U_e^{hf}\right|^2. \#(A20)$$

385 In the terms $\langle T\rangle_b, \langle T\rangle_c, \langle T\rangle_d, \langle T\rangle_e, \langle T\rangle_f$ the functions Z^{hf} and Y_{H1}^{hf} are used. The Z^{hf}
386 function is broken up into multiple terms as $Z^{hf} = Z_1^{hf} + Z_2^{hf} + Z_3^{hf} + Z_4^{hf}$, where

$$Z_1^{hf} = \frac{2\pi i k_\parallel^*}{k_{hf,\parallel}k_\parallel}\sum_{n,x}\int dv_\perp v_\perp J_x\left(k_{hf,\perp}\rho_e\right)J_n(k_\perp\rho_e)J_{n+x}\left(\rho_e\left[k_\perp + k_{hf,\perp}\right]\right) \cdot \int dv_\parallel \frac{1}{\left\{v_\parallel - y_n^{lf}\right\}\left\{v_\parallel - y_x^{hf}\right\}}\frac{\partial f_0(v_\perp, v_\parallel)}{\partial v_\parallel},$$

$$\#(A21)$$

$$Z_2^{hf} = \frac{2\pi i\Omega_{ce}}{k_\parallel k_{hf,\parallel}}\frac{k_\perp^*}{k_\perp}\sum_{n,x} n\int dv_\perp J_x\left(k_{hf,\perp}\rho_e\right)J_n(k_\perp\rho_e)J_{n+x}\left(\rho_e\left[k_\perp + k_{hf,\perp}\right]\right) \cdot \int dv_\parallel \frac{1}{\left\{v_\parallel - y_n^{lf}\right\}\left\{v_\parallel - y_x^{hf}\right\}}\frac{\partial f_0(v_\perp, v_\parallel)}{\partial v_\perp},$$

$$\#(A22)$$

$$Z_3^{hf} = \frac{2\pi i k_\parallel^*}{k_\parallel k_{hf,\parallel}}\sum_{n,x}\int dv_\perp v_\perp J_n(k_\perp\rho_e)J_x\left(k_{hf,\perp}\rho_e\right)J_{n+x}\left(\rho_e\left[k_\perp + k_{hf,\perp}\right]\right) \cdot \int dv_\parallel \frac{f_0(v_\perp, v_\parallel)}{\left\{v_\parallel - y_n^{lf}\right\}\left\{v_\parallel - y_x^{hf}\right\}^2},$$

$$\#(A23)$$

$$Z_4^{hf} = \frac{i\pi}{k_\parallel}\frac{k_{hf,\perp}}{k_{hf,\parallel}}\frac{k_\perp^*}{k_\perp}\sum_{n,x} n\int dv_\perp J_n(k_\perp\rho_e)\left[J_x\left(k_{hf,\perp}\rho_e\right)J_{n+x-1}\left(\rho_e\left[k_\perp + k_{hf,\perp}\right]\right)\right.$$
$$\left. - J_x\left(k_{hf,\perp}\rho_e\right)J_{n+x+1}\left(\rho_e\left[k_\perp + k_{hf,\perp}\right]\right)\right.$$
$$\left. + \left(J_{x-1}\left(k_{hf,\perp}\rho_e\right) - J_{x+1}\left(k_{hf,\perp}\rho_e\right)\right)J_{n+x}\left(\rho_e\left[k_\perp + k_{hf,\perp}\right]\right)\right]$$
$$\cdot \int dv_\parallel \frac{f_0(v_\perp, v_\parallel)}{\left\{v_\parallel - y_n^{lf}\right\}\left\{v_\parallel - y_x^{hf}\right\}}.$$

$$\#(A24)$$

387 Finally, the Y_{H1}^{hf} function is broken up as

$$Y_{H1}^{hf} = \frac{1}{1 + H_1^{hf}}\left(\nu_e Z^{hf} + Y_{Y1}^{hf} + Y_{Y2}^{hf} + Y_{Y3}^{hf} + Y_{Y4}^{hf}\right). \#(A25)$$

388 Where H_1^{hf} is the susceptibility at high frequencies, defined as

$$H_1^{hf}\left[\omega_{hf}, k_{hf}\right] = \left(1 + U_e^{hf}\left[\omega_{hf}, k_{hf}\right]\right)\chi_e^{hf}\left[\omega_{hf}, k_{hf}\right] + U_e^{hf}\left[\omega_{hf}, k_{hf}\right]. \#(A26)$$

Appendix B provides the equations for $U_e^{hf}\left[\omega_{hf}, k_{hf}\right]$ and $\chi_e^{hf}\left[\omega_{hf}, k_{hf}\right]$. The four remaining terms in Equation A23 are

$$Y_{Y1}^{hf} = \frac{\omega_{pe}^2}{k_{hf}^2}\frac{2\pi k_\parallel^*}{k_{hf,\parallel}k_\parallel}\sum_{n,x}\int dv_\perp v_\perp J_x\left(k_{hf,\perp}\rho_e\right)J_n\left(k_\perp\rho_e\right)J_{n+x}\left(\rho_e\left[k_\perp + k_{hf,\perp}\right]\right)$$
$$\cdot\int dv_\parallel \frac{1}{\left\{v_\parallel - y_n^{lf}\right\}\left\{v_\parallel - y_x^{hf}\right\}}\left[k_{hf,\parallel}\frac{\partial^2 f_0(v_\perp, v_\parallel)}{\partial v_\parallel^2} + \frac{x\Omega_{ce}}{v_\perp}\frac{\partial^2 f_0(v_\perp, v_\parallel)}{\partial v_\parallel \partial v_\perp}\right], \quad \#(A27)$$

$$Y_{Y2}^{hf} = \frac{\omega_{pe}^2}{k_{hf}^2}\frac{2\pi\Omega_{ce}}{k_\parallel k_{hf,\parallel}}\frac{k_\perp^*}{k_\perp}\sum_{n,x} n\int dv_\perp J_x\left(k_{hf,\perp}\rho_e\right)J_n\left(k_\perp\rho_e\right)J_{n+x}\left(\rho_e\left[k_\perp + k_{hf,\perp}\right]\right)$$
$$\cdot\int dv_\parallel \frac{1}{\left\{v_\parallel - y_n^{lf}\right\}\left\{v_\parallel - y_x^{hf}\right\}}\left[k_{hf,\parallel}\frac{\partial^2 f_0(v_\perp, v_\parallel)}{\partial v_\parallel \partial v_\perp} + \frac{x\Omega_{ce}}{v_\perp}\frac{\partial^2 f_0(v_\perp, v_\parallel)}{\partial v_\perp^2}\right], \quad \#(A28)$$

$$Y_{Y3}^{hf} = \frac{\omega_{pe}^2}{k_{hf}^2}\frac{2\pi k_\parallel^*}{k_\parallel k_{hf,\parallel}}\sum_{n,x}\int dv_\perp v_\perp J_n\left(k_\perp\rho_e\right)J_x\left(k_{hf,\perp}\rho_e\right)J_{n+x}\left(\rho_e\left[k_\perp + k_{hf,\perp}\right]\right)$$
$$\cdot\int dv_\parallel \frac{1}{\left\{v_\parallel - y_n^{lf}\right\}\left\{v_\parallel - y_x^{hf}\right\}^2}\left[k_{hf,\parallel}\frac{\partial f_0(v_\perp, v_\parallel)}{\partial v_\parallel} + \frac{x\Omega_{ce}}{v_\perp}\frac{\partial f_0(v_\perp, v_\parallel)}{\partial v_\perp}\right], \quad \#(A29)$$

$$Y_{Y4}^{hf} = \frac{\omega_{pe}^2}{k_{hf}^2}\frac{\pi}{k_\parallel}\frac{k_{hf,\perp}}{k_{hf,\parallel}}\frac{k_\perp^*}{k_\perp}\sum_{n,x} n\int dv_\perp J_n\left(k_\perp\rho_e\right)\left[J_x\left(k_{hf,\perp}\rho_e\right)J_{n+x-1}\left(\rho_e\left[k_\perp + k_{hf,\perp}\right]\right)\right.$$
$$- J_x\left(k_{hf,\perp}\rho_e\right)J_{n+x+1}\left(\rho_e\left[k_\perp + k_{hf,\perp}\right]\right)$$
$$\left. + \left(J_{x-1}\left(k_{hf,\perp}\rho_e\right) - J_{x+1}\left(k_{hf,\perp}\rho_e\right)\right)J_{n+x}\left(\rho_e\left[k_\perp + k_{hf,\perp}\right]\right)\right]$$
$$\cdot\int dv_\parallel \frac{1}{\left\{v_\parallel - y_n^{lf}\right\}\left\{v_\parallel - y_x^{hf}\right\}}\left[k_{hf,\parallel}\frac{\partial f_0(v_\perp, v_\parallel)}{\partial v_\parallel} + \frac{x\Omega_{ce}}{v_\perp}\frac{\partial f_0(v_\perp, v_\parallel)}{\partial v_\perp}\right]. \quad \#(A30)$$

Appendix B: Standard Linear Terms

The linear terms from Equation 39 define the standard solution for the ion-acoustic mode (low frequencies), and the derivation of these terms is found in *Froula et al*. (2011). In the magnetized, collisional regime for species *s*, these terms are

$$U_s = i\sum_n e^{-k_\perp^2\bar{\rho}_s^2} I_n\left(k_\perp^2\bar{\rho}_s^2\right)\frac{\nu_{cs}}{\omega - n\Omega_s - i\nu_{cs}} Z_s\left[\frac{\omega - n\Omega_s - i\nu_{cs}}{k_\parallel v_{th,s}}\right], \#(B1)$$

$$\chi_s = \alpha^2 \left(1 + \frac{i\omega}{\nu_{cs}} \frac{U_s}{1+U_s}\right), \#(B2)$$

$$M_s = -\frac{1}{\nu_{cs}|1+U_s|^2} (\mathrm{Re}[U_s] + |U_s|^2). \#(B4)$$

where $v_{th,s} = \sqrt{2KT_s/m_s}$, and I_n is the modified Bessel function. The average gyroradius is

$$\bar{\rho}_s = \frac{v_{th,s}}{\sqrt{2}\,\Omega_s}. \#(B4)$$

Z_s is the usual plasma dispersion function (also called the Dawson or Faddeeva function), which for Maxwellian distributions is

$$Z_s[x] = 2x\, e^{-x^2} \left(\int_0^x e^{s^2} ds + i\sqrt{\pi}\right). \#(B5)$$

For terms evaluated at high frequencies (ω_{hf} and ω^*), only the electron components are needed. These terms are derived in *Longley et al.* (2021). The terms are separated into thermal (m) and suprathermal (h) components, so that the dielectric function is

$$\epsilon^{hf}\left[\omega_{hf}, k_{hf}\right] = 1 + \chi_m^{hf}\left[\omega_{hf}, k_{hf}\right] + \chi_h^{hf}\left[\omega_{hf}, k_{hf}\right]. \#(B6)$$

The real and imaginary parts of the susceptibilities are

$$\mathrm{Re}\left[\chi_m^{hf}\right] = \alpha^2 \left(1 - \frac{\omega}{k_\parallel v_{th,m}} \sum_l e^{-k_\perp^2 \bar{\rho}_m^2} I_l(k_\perp^2 \bar{\rho}_m^2)(2\mathrm{Daw}[y_l])\right) - \frac{\alpha^2 \nu_m}{k_\parallel v_{th,m}} \left\{\sum_l e^{-k_\perp^2 \bar{\rho}_m^2} I_l(k_\perp^2 \bar{\rho}_m^2) \left(2\sqrt{\pi}(1 - y_l x_0) e^{-y_l^2}\right)\right\}, \#(B7)$$

$$\mathrm{Im}\left[\chi_m^{hf}\right] = -\frac{\alpha^2 \omega}{k_\parallel v_{th,m}} \sum_l \left[e^{-k_\perp^2 \bar{\rho}_m^2} I_l(k_\perp^2 \bar{\rho}_m^2) \sqrt{\pi} e^{-y_l^2}\right] + \frac{\alpha^2 \nu_m}{k_\parallel v_{th,m}} \left\{\sum_l e^{-k_\perp^2 \bar{\rho}_m^2} I_l(k_\perp^2 \bar{\rho}_m^2) \left(4(1 - y_l x_0)\mathrm{Daw}[y_l] - \left(\frac{1}{x_0} - 2x_0\right)\right)\right\}, \#(B8)$$

$$\mathrm{Re}\left[\chi_h^{hf}\right] = -2\pi \frac{\omega_p^2}{k^2 k_\parallel} \left(\frac{n_{0h}}{n_{0m}}\right) \sum_l \int_0^\infty dv_\perp v_\perp J_l^2 \left(k_\perp \frac{v_\perp}{\Omega_c}\right) \cdot \left(\frac{l\Omega}{v_\perp} \mathcal{P} \int_{-\infty}^\infty dv_\parallel \frac{\frac{\partial f_{0h}}{\partial v_\perp}}{v_\parallel - \frac{\omega - l\Omega}{k_\parallel}} + k_\parallel \mathcal{P} \int_{-\infty}^\infty dv_\parallel \frac{\partial f_{0h}/\partial v_\parallel}{v_\parallel - \frac{\omega - l\Omega_c}{k_\parallel}}\right), \#(B9)$$

$$\mathrm{Im}\left[\chi_h^{hf}\right] = 2\pi^2 \frac{\omega_p^2}{k^2 k_\parallel}\left(\frac{n_{0h}}{n_{0m}}\right)\sum_l \int_0^\infty dv_\perp v_\perp J_l^2\left(k_\perp \frac{v_\perp}{\Omega_c}\right)\left(\frac{l\Omega}{v_\perp}\left[\frac{\partial f_{0h}}{\partial v_\perp}\right]_{v_\parallel=\frac{\omega-l\Omega}{k_\parallel}} + k_\parallel\left[\frac{\partial f_{0h}}{\partial v_\parallel}\right]_{v_\parallel=\frac{\omega-l\Omega}{k_\parallel}}\right).$$

$$\#(B10)$$

In practice, using Equations B1 – B5 creates difficulties for aspect angles nearly perpendicular to the magnetic field. The linear theory in *Froula et al.* (2011) uses a BGK collision operator, which does not adequately model Coulomb collisions and their effect on ion-cyclotron resonances. Equations B1 – B5 will therefore lead to oscillating structures of the ion-acoustic mode for angles within ≈ 10° of perpendicular to B (see *Kudeki and Milla*, 2011; *Milla and Kudeki*, 2011; and *Longley et al.*, 2019). For the low-frequency linear terms we use the theory from *Kudeki and Milla* (2011), which models Coulomb collisions as a Brownian collision operator.

In the *Kudeki and Milla* (2011) framework, the distribution and susceptibility terms are

$$M_s = 2N\mathrm{Re}[J_s(\omega_s)]\#(B11)$$

$$\chi_s = \frac{1}{k^2\lambda_d^2}(1 - i\omega J_s)\#(B12)$$

The Gordeyev integral J_s is defined as

$$J_s(\omega) = \int_0^\infty d\tau e^{i\omega\tau}\left\langle e^{i\vec{k}\cdot\Delta\vec{r}}\right\rangle \#(B13)$$

And the autocorrelation function in a magnetized plasma with a Brownian collision operator was worked out in *Woodman* (1967):

$$\left\langle e^{i\vec{k}\cdot\Delta\vec{r}}\right\rangle = \exp\left[-k_\parallel^2\frac{c_s^2}{\nu_{cs}^2}(\nu_{cs}\tau - 1 + e^{\nu_s\tau})\right] \cdot \exp\left[-k_\perp^2\frac{c_s^2}{\nu_s^2+\Omega_s^2}(\cos(2\gamma) + \nu_s\tau - e^{\nu_s\tau}\cos(\Omega_s\tau - 2\gamma))\right]$$

$$\#(B14)$$

where ν_s is the constant collision rate for the Brownian collision operator, and $\gamma \equiv \arctan(\nu_s/\Omega_s)$.

Acknowledgments

The author thanks Lindsay Goodwin, Alex Green, and Meers Oppenheim for suggested revisions to this manuscript. This research was supported by NASA LWS grant 80NSSC21K1322, and by the NASA LWS Jack Eddy Postdoctoral Fellowship Program, administered by UCAR's CPAESS under award NNX16AK22G. We thank the International Space Science Institute for facilitating discussions related to this paper as part of the International Team "An Exploration of the Valley Region in the Low Latitude Ionosphere."

Open Research

The code used to generate the figures in this paper is available at https://zenodo.org/doi/10.5281/zenodo.10003668

References

Chau, J. L., and E. Kudeki, (2013). Discovery of two distinct types of equatorial 150 km radar echoes. Geophysical Research Letters, 40, 4509–4514. doi:10.1002/grl.50893

Chau, J. L., W. J. Longley, P. M. Reyes, N. M. Pedatella, Y. Otsuka, C. Stolle, H. Liu, S. L. England, M. A. Milla, D. L. Hysell, M. M. Oppenheim, A. Patra, G. Lehmacher, and E. Kudeki (2023), Solved and unsolved riddles about low-latitude daytime valley region plasma waves and 150-km echoes. Front. Astron. Space Sci. doi:10.3389/fspas.2023.1091319

Derghazarian, S., Hysell, D. L., Kuyeng, K., & Milla, M. A. (2021). High altitude echoes from the equatorial topside ionosphere during solar minimum. Journal of Geophysical Research: Space Physics, 126, e2020JA028424. https://doi.org/10.1029/2020JA028424

Derghazarian, S., Rojas, E. L., Hysell, D. L., & Seyler, C. E. (2023). Lower hybrid waves in high altitude echoes of the topside equatorial ionosphere. Journal of Geophysical Research: Space Physics, 128, e2022JA031036. https://doi.org/10.1029/2022JA031036

Green, Alexander, Meers M. Oppenheim, William J. Longley, (2023) Evaluating the Upper Hybrid Instability as a Cause for 150 km Echoes. J. Geophys. Res. Space Physics. 128, e2022JA031223. doi:10.1029/2022JA031223

Froula, D. H., S. H. Glenzer, N. C. Luhmann Jr., and J. Sheffield (2011), Plasma Scattering of Electromagnetic Radiation: Theory and Measurement Techniques. Burlington, MA: Academic Press. doi:10.1016/B978-0-12-374877-5.00001-4

Kudeki, E., & Fawcett, C. D. (1993). High resolution observations of 150 km echoes at Jicamarca. Geophysical Research Letters, 20, 1987–1990. doi:10.1029/93GL01256

Kudeki, E., and M. Milla (2011), Incoherent scatter spectral theories part I: A general framework and results for small magnetic aspect angles. IEEE Trans. Geosci. Remote Sens., 49(1), 315–328. doi: 10.1109/TGRS.2010.2057252

Lehmacher, G. A., Wu, H., Kudeki, E., Reyes, P. M., Hysell, D. L., & Milla, M. (2020). Height variation of gaps in 150-km echoes and Whole Atmosphere Community Climate Model electron densities suggest link to upper hybrid resonance. Journal of Geophysical Research: Space Physics, 125(1), 125. doi:10.1029/2019JA027204

Longley, W. J., Meers M. Oppenheim, Yakov S. Dimant, (2019). Nonlinear effects of electron-electron collisions on ISR temperature measurements. J. Geophys. Res. Space Physics, doi:10.1002/2019JA026753

Longley, William J., Meers M. Oppenheim, Nick M. Pedatella, Yakov S. Dimant, (2020). The photoelectron driven upper hybrid instability as the cause of 150 km echoes. Geophys. Res. Lett., 47. doi: 10.1029/2020GL087391

Longley, William J., Juha Vierinen, Mike P. Sulzer, Phil J. Erickson, Roger H. Varney, Phil Perillat, (2021) An explanation for Arecibo plasma line power striations. J. Geophys. Res. Space Physics, 126, e2020JA028734. doi: 10.1029/2020JA028734

Milla, M., and E. Kudeki (2011), Incoherent scatter spectral theories part II: Modeling the spectrum for modes propagating perpendicular to B. IEEE Trans. Geosci. Remote Sens., 49(1), 329–345. doi:10.1109/TGRS.2010.2057253

Nicholson, D. R. (1983). Introduction to plasma theory. New York, NY: Wiley.

Oppenheim, M. M., & Dimant, Y. S. (2016). Photoelectron-induced waves: A likely source of 150 km radar echoes and enhanced electron modes. Geophysical Research Letters, 43, 3637–3644. doi:10.1002/2016GL068179

Patra, A. K., Chaitanya, P. P., Rao, M. D., & Kamaraj, P. (2020a). Common-volume dual-frequency radar observations of 150-km echoes and implications. Journal of Geophysical Research: Space Physics, 125, e2019JA027317. https://doi.org/10.1029/2019JA027317

Patra, A. K., Chaitanya, P. P., Rao, M. D., & Reddy, G. J. (2020b). On the Type-A and Type-B 150-km radar echoes. Journal of Geophysical Research: Space Physics, 125, e2020JA028551. https://doi.org/10.1029/2020JA028551

Woodman, R. F. (1967), Incoherent scattering of electromagnetic waves by a plasma, Ph.D. dissertation, Harvard Univ., Cambridge, MA, Mar. 1967.